Structural study on Ni nanowires in an anodic alumina membrane by using *in situ* heating extended x-ray absorption fine structure and x-ray diffraction techniques

2008 J. Phys.: Condens. Matter 20 115205

(http://iopscience.iop.org/0953-8984/20/11/115205)

IOP Publishing Journal of Physics: Condensed Matter

J. Phys.: Condens. Matter **20** (2008) 115205 (7pp) doi:10.1088/0953-8984/20/11/115205

Structural study on Ni nanowires in an anodic alumina membrane by using *in situ* heating extended x-ray absorption fine structure and x-ray diffraction techniques

Quan Cai[1,2], Junxi Zhang[3], Xing Chen[1,2], Zhongjun Chen[1], Wei Wang[1,2], Guang Mo[1,2], Zhonghua Wu[1,2,5], Lide Zhang[3] and Wei Pan[4]

[1] Beijing Synchrotron Radiation Facility, Institute of High Energy Physics, Chinese Academy of Sciences, Beijing 100049, People's Republic of China
[2] Graduate University of Chinese Academy of Sciences, Beijing 100049, People's Republic of China
[3] Institute of Solid State Physics, Chinese Academy of Sciences, Hefei 230031, People's Republic of China
[4] Jiangxi Institute of Measurement and Testing, Nanchang 330002, People's Republic of China

E-mail: wuzh@mail.ihep.ac.cn

Received 13 August 2007, in final form 25 December 2007
Published 20 February 2008
Online at stacks.iop.org/JPhysCM/20/115205

Abstract

Polycrystalline Ni nanowires have been prepared by electrochemical deposition in an anodic alumina membrane template with a nanopore size of about 60 nm. *In situ* heating extended x-ray absorption fine structure and x-ray diffraction techniques are used to probe the atomic structures. The nanowires are identified as being mixtures of nanocrystallites and amorphous phase. The nanocrystallites have the same thermal expansion coefficient, of 1.7×10^{-5} K^{-1}, as Ni bulk; however, the amorphous phase has a much larger thermal expansion coefficient of 3.5×10^{-5} K^{-1}. Details of the Ni nanowire structures are discussed in this paper.

(Some figures in this article are in colour only in the electronic version)

1. Introduction

In recent years, one-dimensional nanomaterial research has been of great interest because of unusual properties and potential applications [1–10]. The practical application of nanomaterials requires keeping steady structures and morphology. With the development of nanodevices, structural change of nanomaterials with temperature deserves more and more attention. Metallic nanowires are important kinds of nanomaterials, and have often been electrochemically deposited into anodic alumina membrane (AAM) templates to form metallic nanowire arrays. Although a lot of metallic nanowires have been well prepared [11–19], as far as we know, few studies on the *in situ* heating structural behaviors [20–22] of metallic nanowires have been reported. Wang *et al* claimed that Cu nanowires in AAM templates have a thermal expansion coefficient close to zero [21], whereas Li reported that Bi nanowire thermal expansion behaviors depend on their diameters [22]. The recent work [20] on single-crystalline Ag nanowires showed two different thermal expansion coefficients in the measurement temperature range. Theoretical simulations [23] demonstrated that compact, helical and amorphous-like structures are presented by Ni nanowires with different wire lengths, and the shape change of Au nanorods [24] is accompanied by a structural change. Even for gold nanoparticles, a negative thermal expansion coefficient [25] was found. However, the microstructure and thermal behaviors of polycrystalline metal nanowires are still ambiguous. In addition, most metal nanowires grown in AAM templates consist of small polyhedral nanocrystallites. X-ray

[5] Author to whom any correspondence should be addressed.

diffraction (XRD) often gave an average nanocrystallite size of less than 40 nm according to Scherrer's equation [26–28], but the nanopore diameter in the AAM template is only one to two nanocrystallite sizes. How the nanocrystallites construct polycrystalline nanowires is an interesting issue.

In this paper, an *in situ* heating study on the structures of polycrystal-like Ni nanowires was performed by using synchrotron radiation, XRD and extended x-ray absorption fine structure (EXAFS) techniques. Combining the short-range sensitive EXAFS technique and the long-range sensitive XRD technique, assisted by high resolution transmission electron microscopy (HRTEM) and scanning electron microscopy (SEM) direct observation, these Ni nanowires' structural changes with temperature are studied.

2. Experiment

The AAM template was prepared by the following two-step procedure. Firstly, annealed and electropolished pure Al foil was anodized in 3 M oxalic acid solution at 15 °C for 4 h as the first step; after removal of the alumina layer using a chemical etch, it was treated in the same conditions as above for 10 h as the second step. Then a quite homogeneous pore distribution was obtained in the AAM template. After eliminating the bottoms of the pores and sputtering a layer of gold, DC electrochemical deposition was performed in Ni sulfate electrolyte (100 g l^{-1} $NiSO_4$, and 30 g l^{-1} H_3BO_4) with the voltage of 2.0 V. Finally, the sample was polished and cut into three pieces, for SEM/HRTEM observation, EXAFS and XRD measurements.

The morphologies of the nanowire arrays were observed with a JEOL S6700 SEM and a JEOL 2010 HRTEM. First, the as-prepared sample was scanned with the SEM to get information on the template. Then, the rate of packing of

the nanopores in the AAM template was observed with SEM after partially dissolving the AAM template in 5% NaOH solution. Finally, the Ni nanowire crystal structure and morphology were identified by using HRTEM after completely removing the AAM template.

The x-ray absorption spectra of the Ni K edge were measured in the transmission mode on the EXAFS station of Beijing Synchrotron Radiation Facility (BSRF). The storage ring was operated at 2.2 GeV with current of about 100 mA. The experiments were carried out at 100, 200, 300, 400, 500 and 600 °C with a temperature fluctuation of ±1 °C under helium atmosphere. At each temperature, the sample was preserved for more then 30 min to reach thermal equilibrium before data collection. The Ni K edge x-ray absorption spectra were collected over 630 eV behind the energy threshold. The thermal couple was set to approach the sample with a space of about 1 mm. The energy resolution ($\Delta E/E$) was about 2×10^{-4} at the Ni K edge, and the harmonics was minimized by detuning the double-crystal Si(111) monochromator to reduce the 70% intensity of the incident x-rays. Considering the length of Ni nanowires to be about 20 μm, and the clearance between nanowires less than 30 nm, the sample was slightly tilted to avoid x-ray leakage from the alumina. Pure Ni foil with 12 coordination atoms at 2.491 Å was used as the reference sample. Its Ni K edge x-ray absorption spectrum was also measured at the room temperature (25 °C).

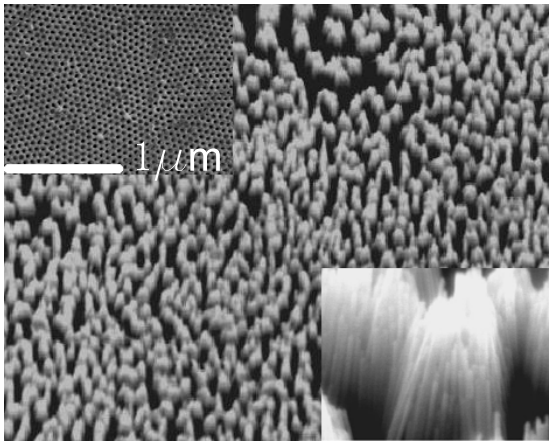

Figure 1. The SEM top view of the sample with removal of the surface layer of the AAM template; Ni nanowires were revealed and gathered into bundles as shown in the lower right inset; an as-prepared sample is shown in the top left inset.

The x-ray diffraction experiments were performed on the XRD station of BSRF and the incident x-ray wavelength was chosen to be 1.54 Å using a double-crystal Si(111) monochromator with the same storage ring conditions as above. The heating process was the same as in the EXAFS measurements. The incident x-ray beam was set approximately parallel to the axial direction of the nanowire. XRD patterns were collected using a curved image plate detector with a diffraction angle accuracy of 0.01° [29]. The diffraction rings were obtained and were transformed into one-dimensional diffraction spectra, which were normalized by the incident x-ray intensity recorded with an ion chamber in front of the sample.

3. Results and discussion

Figure 1 shows the SEM micrograph of the Ni nanowires in the AAM template, from which the top layer was dissolved out. Because of the large slenderness ratio, the dense Ni nanowires are gathered into bundles as shown in the lower right inset. The diameters of nanopores in the AAM template are about 60 nm as shown in the top left inset; all nanopores are arranged hexagonally with a uniform separation of about 90 nm between nanopores.

Figure 2 is the HRTEM image of a single Ni nanowire, in which regular tetrahedral nanocrystallites with average size about 40 nm can be found. There is only one nanocrystallite in the cross section of the nanowire due to the confinement of nanopores in the radial direction. The HRTEM image in the lower left inset taken from the edge of the Ni nanowire shows that the spacing between crystal planes is 0.203 nm, which corresponds to the interplanar distance of (111) planes in face centered cubic (FCC) nickel. This implies that some nanocrystallites in the nanowire have adhered on the inner wall of nanopores with (111) crystal faces. But these nanocrystallites are randomly orientated around the central

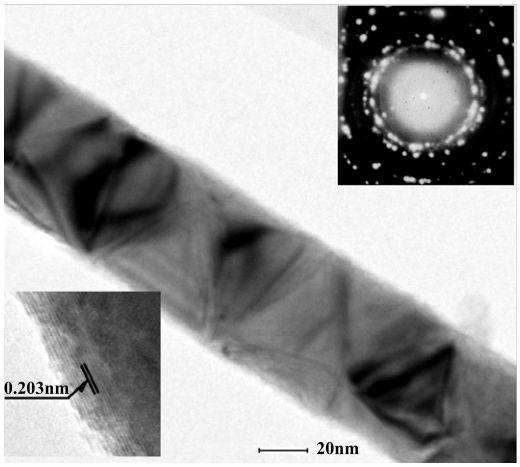

Figure 2. HRTEM image of a single Ni nanowire. Regular tetrahedral nanocrystallites are visible and some nanocrystallites have adhered on the inner wall of the nanopore with (111) crystal planes as shown in the lower left inset. The discrete electron diffraction rings also support a polycrystalline structure of the nanowire as shown in the top right inset.

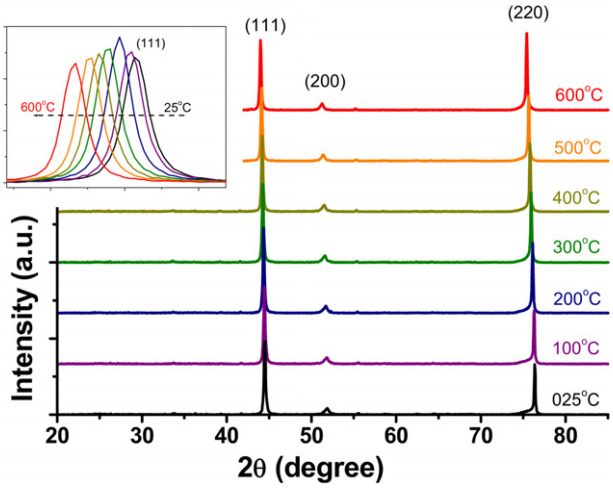

Figure 3. *In situ* heating XRD patterns of Ni nanowires. The peak positions show clearly a lattice expansion. Slightly amorphous contributions can be seen from the bottom of the (220) peaks. The inset compares the peak positions and intensities of the (111) diffraction.

axis of the nanopore to form the polycrystal-like structure as shown by the electron diffraction pattern in the top right inset. The discrete diffraction rings identify the discretization of the nanocrystallite's orientations and a limited number of nanocrystallites in a nanowire.

Figure 3 shows the *in situ* heating XRD patterns of Ni nanowires. All diffraction peaks are in good agreement with those of bulk Ni (ICSD No. 76667) and can be indexed to FCC structure. An asymmetrical bottom of the (220) diffraction indicates the x-ray diffuse scattering contribution, which is probably caused by crystalline defects, partial disorder or amorphous phase. The interplanar distances have been calculated from the XRD patterns as listed in table 1, which are in excellent agreement with those obtained from the electron

Table 1. Structural parameters of Ni nanowires obtained by using *in situ* heating EXAFS and XRD techniques. N, R, σ^2, $\sigma^{(3)}$ and ΔE are, respectively, the coordination number, bond length, Debye–Waller factor, third cumulant and shift of the energy threshold. $d(111)$ and $d(200)$ are the interplanar distances of (111) and (200), respectively.

	EXAFS					XRD	
T (°C)	N	R (Å)	σ^2 (Å^2)	$\sigma^{(3)}$ (Å^3)	ΔE (eV)	$d(111)$ (Å)	$d(200)$ (Å)
25	—	—	—	—	—	2.034	1.761
100	12.0	2.49(6)	0.0017	8.7×10^{-5}	−0.8	2.036	1.762
200	12.0	2.50(0)	0.0032	1.9×10^{-4}	0.2	2.040	1.766
300	12.0	2.50(8)	0.0055	3.4×10^{-4}	−0.6	2.044	1.769
400	12.0	2.51(5)	0.0076	5.2×10^{-4}	−0.7	2.047	1.772
500	11.9	2.52(4)	0.0096	7.2×10^{-4}	0.1	2.050	1.775
600	11.6	2.52(7)	0.0112	9.2×10^{-4}	0.7	2.056	1.780

diffraction patterns. The thermal expansion coefficient of Ni nanocrystallites in the polycrystal-like Ni nanowires is estimated to be 1.7×10^{-5} K^{-1} as in bulk Ni. This is obviously different from the thermal expansion behaviors of other metal nanowires in AAM templates. Single-crystal Cu nanowires [21] were claimed to have no thermal expansion, and this was attributed to the diffusion of vacancy defects from the body to the surface of nanowires. Single-crystal Bi nanowires [22] were reported to have thermal expansion changing with the diameter of the nanowires, while the new work demonstrates that there are two different thermal expansion coefficients for Ag nanowire from room temperature to 800 °C. It is well known that bulk Ni ($\sim 1.7 \times 10^{-5}$ K^{-1}), Cu ($\sim 2.1 \times 10^{-5}$ K^{-1}), Ag ($\sim 1.7 \times 10^{-5}$ K^{-1}) and Bi ($\sim 1.4 \times 10^{-5}$ K^{-1}) are all thermally expansive. Comparing with their respective bulks, nanowires of Cu, Ag and Bi all show different thermal expansion laws, but Ni nanowires in this work present the same thermal expansion coefficient as bulk Ni. This is because all these Cu, Ag and Bi nanowires are single crystalline, but Ni nanowires are polycrystalline. As the metal nanowires are confined in the alumina nanopores, the alumina template with the thermal expansion coefficient $\sim 8.8 \times 10^{-6}$ K^{-1} will produce a radial pressure on the nanowires. Ni, Ag and Cu nanowires all have highly symmetrical FCC structure, which will lead to approximately isotropic thermal behaviors. Therefore, the radial pressure induced by the AAM template suppresses the thermal expansion of single-crystal metal nanowires with highly symmetrical structure. Although Bi nanowires [22] are also in single-crystal states, the hexagonal unit cell in Bi nanowires is anisotropic, which permits an anisotropic lattice expansion. In this case, the radial pressure can be relaxed by the axial expansion, which results in a complex thermal expansion behavior, showing the dependence of the thermal expansion coefficient on the nanowire diameter. As for the Ni nanowires in this paper, Ni nanocrystallites form polycrystal-like structure. There is enough space between Ni nanocrystallites to release the stress from the lattice expansion. This allows the Ni nanocrystallites to expand as bulk, as indicated in figure 3. Therefore, we can conclude that the thermal expansion coefficient of metal nanowires in AAM templates is dependent on the morphology

and the atomic structures. For polycrystalline nanowires, the thermal expansion coefficient of the nanocrystallites is almost the same as that of the corresponding bulk. For single-crystal nanowires with highly symmetrical structure, the thermal expansion coefficient is decreased due to the radial pressure induced by the alumina nanopores. For single-crystal nanowires with low symmetry structure, the thermal expansion shows complex behaviors.

The x-ray diffraction pattern was collected with a curved image plate in the transmission mode. We also notice that the number of x-ray diffraction peaks in figure 3 is less than the number of electron diffraction rings in figure 2. This is because the Ewald sphere in the electron diffraction is approximately a plane and more crystal planes can satisfy the diffraction condition. There is no phase change or obvious impurity phase appearing in the XRD patterns for the entire measurement temperature range. But the (200) diffractions are quite weak and the (220) diffractions are abnormally intense comparing with the bulk Ni XRD pattern. This means that there are several preferential orientations of nanocrystallites in the Ni nanowires.

On the basis of the XRD patterns, the average nanocrystallite size can be estimated with Scherrer's equation to be about 40 nm in the [111] direction at room temperature, which is also confirmed by the HRTEM image as shown in figure 2. With the temperature increasing, the nanocrystallite size increases slightly. The nanocrystallite size is about 44 nm for the nanowires at 600 °C.

The diffraction peaks of crystal plane (111) are compared in the inset of figure 3. It can be found that the diffraction peak width become less with temperature increasing, but the diffraction peak height become greater from room temperature to 200 °C, then less from 200 to 600 °C. In fact, there are two competing factors acting on the degree of order as we heat the nanowires. One is the nanocrystallite size increasing, which decreases the ratio of the surface to volume and increase the static order. The other is the temperature increasing, which increases the thermal disorder. From the inset of figure 3, we know that the static order is dominant for the crystallites below 200 °C, and the thermal disorder overwhelms the static order above 200 °C.

There have been quite a few good quality papers [18, 19] on EXAFS of metallic nanowires, but studies on the *in situ* heating EXAFS of metallic nanowires are scarce. The Ni K edge EXAFS signals were extracted by using the derivative method [30] and were transferred to k-space from energy space by using the formula $E - E_0 = \hbar^2 k^2 / 2m_e$, where the energy threshold (E_0) was chosen as the maximum of the first derivative for the absorption curve, $\hbar$ is Planck's constant and m_e is the electron mass. Figure 4 shows the Fourier transform (FT) spectra with k^3 weight in the range of 1.8–13.0 Å^{-1}. The room temperature FT spectrum of the K edge EXAFS of bulk Ni was also shown in figure 4. It can be seen that the magnitude of the first coordination peaks decreases with temperature increase, showing the disorder increasing. This change of disorder is different from those found in XRD patterns, which is due to the difference in structural sensitivity between XRD and EXAFS techniques. XRD is sensitive to the long-range order structure, depending on the nanocrystallite size in the crystalline phase, whereas EXAFS is sensitive to the local atomic structures with short-range order; the sample may be crystalline, amorphous, or liquid phase—and even gas molecules. Combining XRD and EXAFS results, we know that both the long-range order (static order) and the short-range disorder (thermal disorder) increase with temperature increase, but the critical temperature is around 200 °C. Below the critical temperature, the increase of long-range order with temperature is faster than the increase of short-range disorder with temperature. Above the critical temperature, the former is slower than the latter.

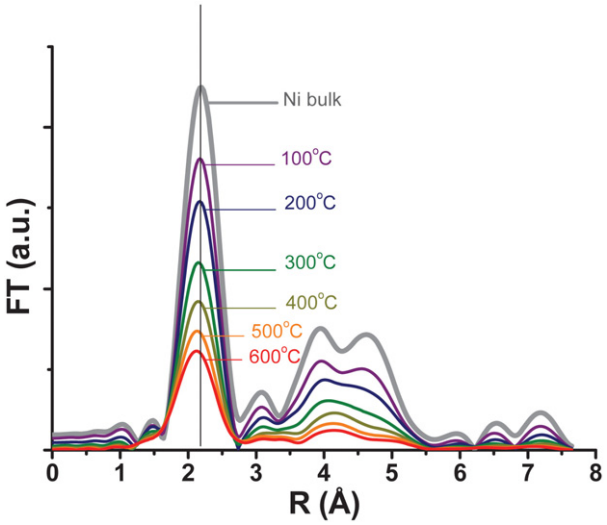

Figure 4. Fourier transform spectra of $k^3\chi(k)$. A guide to the first-shell position is given by the fine line; obviously the peak maximum position shifts to lower values of R and the shape becomes more asymmetrical with temperature increase.

By comparing the FT spectra of the nanowires and the bulk, it is also demonstrated that the nanowires are of FCC structure without any oxidation evidence. From figure 4, it can be found that the maximum value of the first coordination peak shifts toward low R side with temperature increase (the vertical line is a guide). Commonly, this shift may be caused by the bond length contraction or asymmetrical atom pair distribution. But for Ni nanowires, the bond lengths always increase with temperature as indicated by the XRD diffraction shown in figure 3 and table 1. Therefore, an asymmetrical Ni–Ni atom pair model is necessary for describing the local atomic structures.

The first-coordination-shell EXAFS signals of $k^3\chi(k)$ were isolated by using a Hanning window in the range of 1.61–2.76 Å. The EXAFS signals were fitted with the following EXAFS function:

$$\chi_j(k) = \frac{N_j S_0^2}{k r_j^2} F_j(k) e^{-2r_j/\lambda} e^{-2k^2\sigma_j^2} \sin(2kr_j + \phi_j + \Sigma_j)$$

and

$$\Sigma_j = -4\frac{k\sigma_j^2}{r_j} - \frac{4}{3}k^3\sigma_j^{(3)}$$

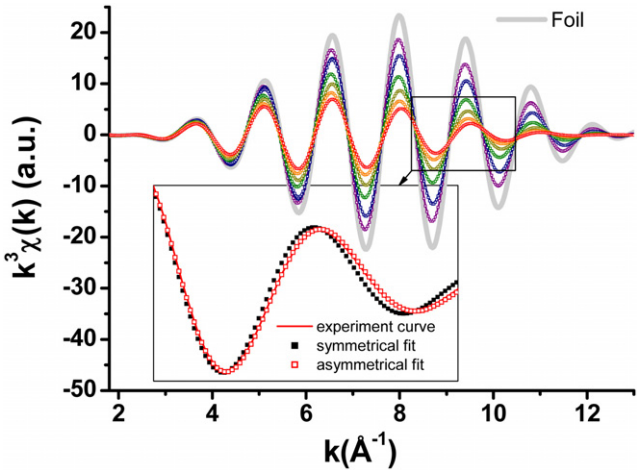

Figure 5. Ni K edge EXAFS spectra of the first coordination shell in Ni nanowires. The hollow dots are the experimental spectra and the solid lines are the asymmetrical model fitting results. The gray wide line is from the Ni foil at 25 °C. The amplitudes decrease with temperature increase for Ni nanowires at 100, 200, 300, 400, 500 and 600 °C. The inset shows a divergence of the symmetrical model from the experimental curve at 600 °C.

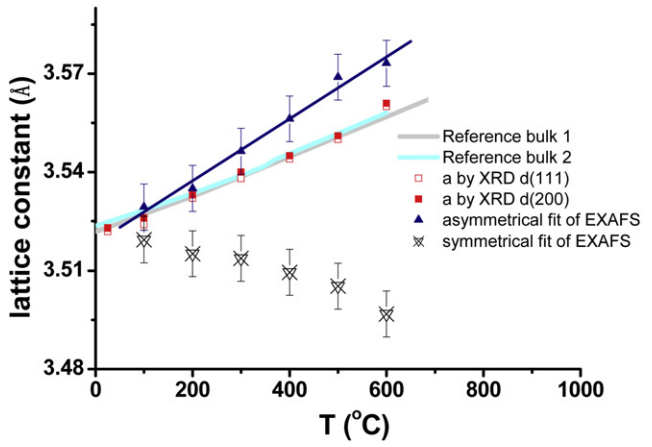

Figure 6. Comparison of the lattice constants. XRD results are in good agreement with the reference bulks. EXAFS results with a symmetrical atom pair model give a negative thermal expansion. A larger thermal expansion compared with bulk Ni is shown with a slightly asymmetrical atom pair model keeping the third cumulant.

where N_j, r_j, σ_j^2 and ΔE_j are, respectively, the coordination number, bond length, Debye–Waller factor and energy threshold shift of the jth coordination shell. $\sigma_j^{(3)}$ is the third cumulant, λ is the mean electron free path, $F(k)$ is the backscattering amplitude and ϕ_j is the phase shift; these were extracted from the K edge EXAFS spectrum of the reference sample (Ni foil) at room temperature (25 °C). The best fitting curves are shown in figure 5. As an example, the fitting curves of the sample at temperature 600 °C with symmetrical and asymmetrical models are compared and shown in the inset of figure 5. Obviously, the symmetrical model cannot give reasonable results due to a large residual. The best fitting parameters obtained with the asymmetrical model are listed in table 1. Finally, the corresponding lattice parameters of the FCC unit cell are calculated by using $a = \sqrt{2}r_1$ as plotted in figure 6.

As shown in figure 6, the lattice parameters of Ni nanocrystallites in the nanowires obtained from XRD patterns are in excellent agreement with those of bulk Ni, keeping a nearly isotropic thermal expansion. However, the EXAFS results show a larger thermal expansion behavior for the Ni nanowires. A linear fit to these bond lengths gives the thermal expansion coefficient as being about 2.7×10^{-5} K^{-1}, which is much larger than the 1.7×10^{-5} K^{-1} for the Ni nanocrystallites obtained from XRD measurement. Fornasini *et al* [31–33] discussed the difference of the interatomic distances obtained from EXAFS and XRD. By taking into account the relative displacement ($\Delta u_\perp$) of atoms in the direction perpendicular to the bond, the connection between the interatomic distances measured from EXAFS (R_{XAFS}) and XRD (R_{XRD}) is given by the formula $R_{\mathrm{XAFS}} - R_{\mathrm{XRD}} = \langle \Delta u_\perp^2 \rangle / (2R_{\mathrm{XRD}})$. This means that the interatomic distances obtained from EXAFS should always be larger than those obtained from XRD. They also introduce a parameter $\gamma = \langle \Delta u_\perp^2 \rangle / \langle \Delta u_\parallel^2 \rangle$, where $\Delta u_\parallel$ is the displacement of atoms parallel to bonds and can be approximately replaced by σ^2_{XAFS}. According to this approach, the γ value was estimated to be about 5 for the Ni nanowires in this paper. However, we cannot find a reliable explanation for this much larger γ value. In fact, for a nearly isotropic system, for example, FCC structure, a detailed calculation tells us that the γ value should be between 1 and 2. This causes a bond length increase of less than 0.005 Å between EXAFS and XRD even at 600 °C. Evidently, this is not enough to compensate for the bond length change obtained from EXAFS and XRD; it can even be neglected in our case. Although the EXAFS technique might give a larger interatomic distance than the XRD technique, the difference of interatomic distances obtained from EXAFS and XRD cannot entirely be attributed to the different experimental techniques (EXAFS and XRD) used to study the Ni nanowires in this paper.

A reasonable explanation is that the Ni nanowires contain not only crystallites, but also amorphous contents. It is very general that the interface between two crystallites is a liquid-like phase [34]. Theoretical simulation [23] also demonstrated that an amorphous-like structure gradually develops when the length of Ni nanowire is compressed more. LEED experiments [35] indicated that the surface thermal expansion coefficient of Ni(001) reaches a value nearly 20 times larger than that for the bulk. This confirms not only a large anharmonicity in the interatomic potential on the metal surface, but also a surface disordering transition. Therefore, we believe that the Ni nanowire is a mixture of crystallites and an amorphous phase. Because the Ni nanocrystallite size is about 40 nm, the fraction of the crystalline component in the nanowires can be simply estimated as follows: assuming all Ni nanocrystallites to form a cylinder with a diameter of 40 nm, the nanocrystallites make up about 44% of the volume of one nanowire; the amorphous content occupies 56% of the volume. Even considering the error of the nanocrystallite size, the amorphous content is still more than 50%. Here we take crystallites having the same thermal expansion coefficient 1.7×10^{-5} K^{-1}, as indicated by the XRD results; then the

amorphous content can be approximately estimated as having a thermal expansion coefficient of 3.5×10^{-5} K^{-1}. In fact, the EXAFS technique gave an average result of thermal expansion, between the crystallites and the amorphous content, as shown in figure 6.

Although the amorphous content may have a non-legitimate thermal expansion coefficient because of the disorder structures [21, 22, 25], the amount of atoms in the surface/interface is less than 3.5% [36] for a nanocrystallite larger than 30 nm. For nanocrystallites smaller than 10 nm, structural disorder is often caused by the large ratio of surface/interface to volume [34]. The atoms located at the surface/interface of nanocrystallites show more disorder or even different bond lengths because of the difference in coordination environments from the interior atoms. However, for nanocrystallites larger than 40 nm, the surface/interface layer contains only a few per cent of the total atoms, which is not enough to cause so much variation in the average thermal expansion coefficient of the Ni nanowires. Therefore, the amorphous component in the Ni nanowires has formed amorphous regions, and the amorphous regions are filled into the gaps between the tetrahedral Ni nanocrystallites.

According to the growth mechanism [9, 16] of nanowires in AAM, at the very beginning of polycrystalline nanowire deposition, Ni nanocrystallites are randomly nucleated at the inner wall of the alumina nanopores, and in the course of growth, adjacent nuclei competing makes some of them grow faster and others restrained in growth. Only those nuclei with size larger than a critical size can be grown further. Figure 2 demonstrates that some of the nanocrystallites adhered to the inner wall of alumina nanopores with (111) planes. Because the surface energy of the (111) plane is lowest in the FCC structure, the nanocrystallites appear in the (111) planes as surfaces and form a tetrahedron-like shape. With the growth of the nanocrystallites, their size was restricted by the nanopore dimension, which leads to the nanocrystallite size always being smaller than the nanopore diameter as shown by the HRTEM and XRD results as well as the previous reports. In addition, the crystal lattices of random nucleating tetrahedra do not match each other, which results in a great number of vacancies and voids being left between tetrahedral nanocrystallites. Some nuclei with size smaller than the critical size were aborted and consisted of a few atoms, which were filled into the interstitial space and present no structural periodicity. Theoretical calculation and experimental measurements also show us that atoms in small clusters are often in great disorder, and get the lowest energy and relax the structural stress [37–39]. It was these aborted nuclei that were left in the interstitial space from the amorphous regions in the Ni nanowires, instead of a simple amorphous layer wrapped on the surface of the nanocrystallite.

In situ heating of the Ni nanowires differs from sintering the nanoparticles in a free environment [40]. Here, the Ni nanowires are isolated by the alumina and are restricted in the nanopores; there is no possibility for one nanowire to coalesce with the others. At the same time, the alumina template can partially protect the Ni nanowires from oxidization. In this case, the growth of Ni nanocrystallites and their structural changes are strictly confined within one nanowire. Surrounded by amorphous phase, Ni nanocrystallites cannot coalesce with each other and there is no room for them to contact directly, align or rearrange atoms in the lattice [41]. But these nanocrystallites could be slowly grown with an interface growth mode through atomic diffusion from the amorphous phase to the boundary. Such a process depends on the heating temperature. For the Ni nanowires, the heating temperature is far below their melting point.

4. Conclusion

Polycrystalline Ni nanowires have been prepared by using electrochemical deposition. The atomic structures, morphology and thermal expansion coefficient were studied by using SEM/HRTEM, and *in situ* heating XRD and EXAFS techniques. We believe that this study is helpful for understanding the formation mechanism, the thermal behavior and the applications of nanomaterials. The conclusions can be summarized as follows.

Static order (nanocrystallite size) and thermal disorder (temperature) are two competing factors and both are enhanced with temperature increase. For the Ni nanowires, 200 °C is a transition point; the static order is dominant below 200 °C, but the thermal disorder takes precedence above 200 °C.

The Ni nanowires are a mixture of nanocrystallites and amorphous phase. The Ni nanocrystallite size is about 40 nm, with tetrahedral shape. The phase change from amorphous to crystalline is slow, and Ni nanocrystallite size shows little increase with heating temperature increase.

The average thermal expansion coefficient is dependent on the morphology and structures of metal nanowires. For nanocrystallites, the thermal expansion coefficient is almost the same as that of the corresponding bulk, but for restricted single crystal of nanowire, the thermal expansion could be suppressed (isotropic structure) or become complex (anisotropic structure) in certain temperature ranges.

The polycrystalline Ni nanowires have an average thermal expansion coefficient of 2.7×10^{-5} K^{-1}. Here, the Ni nanocrystallites have the same thermal expansion coefficient, of 1.7×10^{-5} K^{-1}, as bulk Ni, and Ni amorphous phase has a novel thermal expansion coefficient of 3.5×10^{-5} K^{-1}.

Acknowledgments

This work was supported by the National Natural Scientific Foundation of China, No. 10374087, and the Knowledge Innovation Program of the Chinese Academy of Sciences (KJCX3-SYW-N8).

References

[1] Ferré R, Ounadjela K, George J M, Piraux L and Dubois S 1997 *Phys. Rev.* B **56** 14066
[2] Meier J, Doudin B and Ansermet J Ph 1996 *J. Appl. Phys.* **79** 6010
[3] Ounadjela K, Ferré R, Louail L, George J M, Maurice J L, Piraux L and Dubois S 1997 *J. Appl. Phys.* **81** 5455
[4] Pignard S, Goglio G, Radulescu A, Pirauxa L, Dubois S, Declémy A and Duvail J L 2000 *J. Appl. Phys.* **87** 824

[5] Zeng H, Skomski R, Menon L, Liu Y, Bandyopadhyay S and Sellmyer D J 2002 *Phys. Rev.* B **65** 134426
[6] Jin C G, Liu W F, Jia C, Xiang X Q, Cai W L, Yao L Z and Li X G 2003 *J. Cryst. Growth* **258** 337
[7] Jorritsma J and Mydosh J A 1998 *J. Appl. Phys.* **84** 901
[8] Lok J G S, Geim A K, Maan J C, Dubonos S V, Theil Kuhn L and Lindelof P E 1998 *Phys. Rev.* B **58** 12201
[9] Pan H, Liu B, Yi J, Poh C, Lim S, Ding J, Feng Y, Huan C H A and Lin J 2005 *J. Phys. Chem.* B **109** 3094
[10] Tian F, Zhu J and Wei D 2007 *J. Phys. Chem.* C **111** 6994
[11] He H and Tao N J 2003 *Electrochemical Fabrication of Metal Nanowires, Encyclopedia of Nanoscience and Nanotechnology* vol X (California: American Scientific Publishers) pp 1–18
[12] Li A P, Müller F, Birner A, Nielsch K and Gösele U 1998 *J. Appl. Phys.* **84** 6023
[13] Martin C R 1996 *Chem. Mater.* **8** 1739
[14] Sander M S and Tan L-S 2003 *Adv. Funct. Mater.* **13** 393
[15] Wang X W, Fei G T, Xu X J, Jin Z and Zhang L D 2005 *J. Phys. Chem.* B **109** 24326
[16] Tian M, Wang J, Kurtz J, Mallouk T E and Chan M H W 2003 *Nano Lett.* **3** 919
[17] Riveros G, Gomez H, Cortes A, Marotti R E and Dalchiele E A 2005 *Appl. Phys.* A **81** 17
[18] Benfield R E, Grandjean D, Dore J C, Wu Z, Kroll M, Sawitowski T and Schmid G 2001 *Euro. Phys. J.* D **16** 399
[19] Benfield R E, Grandjean D, Dore J C, Esfahanian H, Wu Z, Krol M, Geerkense M and Schmid G 2004 *Faraday Discuss.* **125** 327
[20] Xu X, Fei G, Yu W, Chen L, Zhang L, Ju X, Hao X and Wang B 2006 *Appl. Phys. Lett.* **88** 211902
[21] Wang Y, Yang J, Ye C, Fang X and Zhang L 2004 *Nanotechnology* **15** 1437
[22] Li L, Zhang Y, Yang Y W, Huang X H, Li G H and Zhang L D 2005 *Appl. Phys. Lett* **87** 031912
[23] Zhang H Y, Gu X, Zhang X H, Ye X and Gong X G 2004 *Phys. Lett.* A **331** 332
[24] Wang Y and Dellago C 2003 *J. Phys. Chem.* B **107** 9214
[25] Li W H, Wu S Y, Yang C C, Lai S K, Lee K C, Huang H L and Yang H D 2002 *Phys. Rev. Lett.* **89** 135504
[26] Nielsch K, Wehrspohn R B, Fischer S F, Kronmüller H, Barthel J, Kirschner J and Gösele U 2001 *Mater. Res. Soc. Symp. Proc.* **636** (D1.9.1)
[27] Nielsch K, Wehrspohn R B, Barthel J, Kirschner J, Gösele U, Fischer S F and Kronmüller H 2001 *Appl. Phys. Lett.* **79** 1360
[28] Zheng M, Menon L, Zeng H, Liu Y, Bandyopadhyay S, Kirby R D and Sellmyer D J 2000 *Phys. Rev.* B **62** 12282
[29] Chen Z, Wu Z, Sun M, Chen X, Cai Q and Yang S 2005 *High Energy Phys. Nucl. Phys.* **29** 321 (in Chinese)
[30] Hu T D, Xie Y N, Jin Y L and Liu T 1997 *J. Phys.: Condens. Matter* **9** 5507
[31] Fornasini P 2001 *J. Phys.: Condens. Matter* **13** 7859
[32] Fornasini P, Dalba G, Grisenti R, Purans J, Vaccari M, Rocca F and Sanson A 2006 *Nucl. Instrum. Methods* B **246** 180
[33] Beccara S A, Dalba G, Fornasini P, Grisenti R, Pederiva F, Sanson A, Diop D and Rocca F 2003 *Phys. Rev.* B **68** 140301(R)
[34] Gleiter H 2000 *Acta Mater.* **48** 1
[35] Cao Y and Conrad E 1990 *Phys. Rev. Lett.* **65** 2808
[36] Chang J and Johnson E 2005 *Phil. Mag.* **85** 3617
[37] Yang S H, Drabold D A, Adams J B, Ordejón P and Glassford K 1997 *J. Phys.: Condens. Matter* **9** 39
[38] Michaelian K, Rendón N and Garzón I L 1999 *Phys. Rev.* B **60** 2000
[39] Kim Y-W, Lin H-M and Kelly T F 1989 *Acta Metall.* **37** 247
[40] Wang Z L, Petroski J M, Green T C and El-Sayed M A 1998 *J. Phys. Chem.* B **102** 6145
[41] José-Yacamán M, Gutierrez-Wing C, Miki M, Yang D Q, Piyakis K N and Sacher E 2005 *J. Phys. Chem.* B **109** 9703